Numerical study of fermion and boson models with infinite-range random interactions

Wenbo Fu[1] and Subir Sachdev[1,2]
[1]*Department of Physics, Harvard University, Cambridge, Massachusetts 02138, USA*
[2]*Perimeter Institute for Theoretical Physics, Waterloo, Ontario N2L 2Y5, Canada*
(Received 7 April 2016; published 15 July 2016)

We present numerical studies of fermion and boson models with random all-to-all interactions (the Sachdev-Ye-Kitaev models). The high-temperature expansion and exact diagonalization of the N-site fermion model are used to compute the entropy density: our results are consistent with the numerical solution of $N = \infty$ saddle-point equations, and the presence of a nonzero entropy density in the limit of vanishing temperature. The exact-diagonalization results for the fermion Green's function also appear to converge well to the $N = \infty$ solution. For the hard-core boson model, the exact-diagonalization study indicates spin-glass order. Some results on the entanglement entropy and the out-of-time-order correlators are also presented.

DOI: 10.1103/PhysRevB.94.035135

I. INTRODUCTION

Fermion and boson models with infinite-range random interactions were studied in the 1990s and later [1–6] as models of quantum systems with novel non-Fermi-liquid or spin-glass ground states. More recently, it was proposed that such models are holographically connected to the dynamics of AdS_2 horizons of charged black holes [7,8], and remarkable connections have since emerged to topics in quantum chaos and black hole physics [9–16].

The model introduced by Sachdev and Ye [1] was defined on N sites, and each site had particles with M flavors; then the double limit $N \to \infty$, followed by $M \to \infty$, was taken. In such a limit, the random interactions depend on 2 indices, each taking N values. Taking the double limit is challenging in numerical studies, and so they have been restricted to $M = 2$ with increasing values of N [5,6]. It was found that the ground state for $N \to \infty$ at a fixed $M = 2$ was almost certainly a spin glass. So a direct numerical test of the more exotic non-Fermi-liquid states has not so far been possible.

Kitaev [9] has recently introduced an alternative large-N limit in which the random interaction depends upon 4 indices, each taking N values; the saddle-point equations in the $N \to \infty$ limit are the same as those in Ref. [1]. No separate $M \to \infty$ is required, and this is a significant advantage for numerical study. The present paper will study such Sachdev-Ye-Kitaev (SYK) models by exact diagonalization; some additional results will also be obtained in a high-temperature expansion. Our numerical studies will be consistent with the fermionic SYK model displaying a non-Fermi-liquid state which has extensive entropy, and entanglement entropy, in the zero-temperature limit. For the case of the bosonic SYK model, our numerical study indicates spin-glass order: this implies that the analytic study of the large-N limit will require replica symmetry breaking [3].

The outline of this paper is as follows. In Sec. II, we review the large-N solution of the SYK model, and present results on its high-temperature expansion. In Sec. III we present exact-diagonalization results for the fermionic SYK model, while the hard-core boson case is considered later in Sec. V. Section IV contains a few results on out-of-time-order correlators of recent interest.

II. LARGE-N LIMIT FOR FERMIONS

This section will introduce the SYK model for complex fermions, and review its large-N limit. We will obtain expressions for the fermion Green's function and the free-energy density. A high-temperature expansion for these quantities will appear in Sec. II B.

The Hamiltonian of the SYK model is

$$H = \frac{1}{(2N)^{3/2}} \sum_{i,j,k,\ell=1}^{N} J_{ij;k\ell}\, c_i^\dagger c_j^\dagger c_k c_\ell - \mu \sum_i c_i^\dagger c_i, \quad (1)$$

where the $J_{ij;k\ell}$ are complex Gaussian random couplings with zero mean obeying

$$J_{ji;k\ell} = -J_{ij;k\ell}, \quad J_{ij;\ell k} = -J_{ij;k\ell}, \quad J_{k\ell;ij} = J^*_{ij;k\ell}, \quad \overline{|J_{ij;k\ell}|^2} = J^2. \quad (2)$$

The above Hamiltonian can be viewed as a "matrix model" on Fock space, with a dimension which is exponential in N. But notice that there are only order N^4 independent matrix elements, and so Fock space matrix elements are highly correlated. The conserved $U(1)$ density $\mathcal{Q}$ is related to the average fermion number by

$$\mathcal{Q} = \frac{1}{N} \sum_i \langle c_i^\dagger c_i \rangle. \quad (3)$$

The value of $\mathcal{Q}$ can be varied by the chemical potential μ, and ranges between 0 an 1. The solution described below applies for the range of μ for which $0 < \mathcal{Q} < 1$, and so realizes a compressible state.

Using the imaginary-time path-integral formalism, the partition function can be written as

$$\mathcal{Z} = \int Dc^\dagger Dc \exp(-\mathcal{S}), \quad (4)$$

where

$$\mathcal{S} = \int_0^\beta d\tau (c^\dagger \partial_\tau c + H), \quad (5)$$

where $\beta = 1/T$ is the inverse temperature, and we have already changed the operator c into a Grassmann number.

In the replica trick, we take n replicas of the system and then take the $n \to 0$ limit

$$\ln \mathcal{Z} = \lim_{n\to 0} \frac{1}{n}(\mathcal{Z}^n - 1). \tag{6}$$

Introducing replicas c_{ia}, with $a = 1 \ldots n$, we can average over disorder and obtain the replicated imaginary-time (τ) action

$$\mathcal{S}_n = \sum_{ia} \int_0^\beta d\tau c_{ia}^\dagger \left(\frac{\partial}{\partial\tau} - \mu\right) c_{ia} - \frac{J^2}{4N^3} \sum_{ab} \int_0^\beta d\tau d\tau' \left| \sum_i c_{ia}^\dagger(\tau) c_{ib}(\tau') \right|^4 \tag{7}$$

(here we neglect normal-ordering corrections which vanish as $N \to \infty$). Then the partition function can be written as

$$\mathcal{Z}^n = \int \prod_a Dc_a^\dagger Dc_a \exp(-\mathcal{S}_n). \tag{8}$$

Notice that the action has a global SU(N) symmetry under $c_{ia} \to U_{ij} c_{ja}$. Also, if we ignore the time-derivative term in Eq. (7), notice that the action has a $U(1)$ gauge invariance under $c_{ia} \to e^{i\vartheta_i(\tau)} c_{ja}$. And indeed, in the low-energy limit leading to Eq. (19), the time-derivative term can be neglected. However, we cannot drop the time-derivative term at the present early stage, as it plays a role in selecting the manner in which the $U(1)$ gauge invariance is "broken" in the low-energy limit. In passing, we note that this phenomenon appears to be analogous to that described in the holographic study of non-Fermi liquids by DeWolfe *et al.* [17]: there, the bulk fermion representing the low-energy theory is also argued to acquire the color degeneracy of the boundary fermions due to an almost broken gauge invariance. As in Ref. [17], we expect the bulk degrees of freedom of gravitational duals to the SYK model to carry a density of order N [10].

Following the earlier derivation [1], we decouple the interaction by two successive Hubbard-Stratonovich transformations. First, we introduce the real field $Q_{ab}(\tau,\tau')$ obeying

$$Q_{ab}(\tau,\tau') = Q_{ba}(\tau',\tau). \tag{9}$$

The equation above is required because the action is invariant under the reparametrization $a \leftrightarrow b, \tau \leftrightarrow \tau'$. In terms of this field

$$\mathcal{S}_n = \sum_{ia} \int_0^\beta d\tau c_{ia}^\dagger \left(\frac{\partial}{\partial\tau} - \mu\right) c_{ia} + \sum_{ab} \int_0^\beta d\tau d\tau' \left\{ \frac{N}{4J^2} [Q_{ab}(\tau,\tau')]^2 - \frac{1}{2N} Q_{ab}(\tau,\tau') \left| \sum_i c_{ia}^\dagger(\tau) c_{ib}(\tau') \right|^2 \right\}. \tag{10}$$

A second decoupling with the complex field $P_{ab}(\tau,\tau')$ obeying

$$P_{ab}(\tau,\tau') = P_{ba}^*(\tau',\tau) \tag{11}$$

yields

$$\mathcal{S}_n = \sum_{ia} \int_0^\beta d\tau c_{ia}^\dagger \left(\frac{\partial}{\partial\tau} - \mu\right) c_{ia} + \sum_{ab} \int_0^\beta d\tau d\tau' \left\{ \frac{N}{4J^2} [Q_{ab}(\tau,\tau')]^2 + \frac{N}{2} Q_{ab}(\tau,\tau') |P_{ab}(\tau,\tau')|^2 - Q_{ab}(\tau,\tau') P_{ba}(\tau',\tau) \sum_i c_{ia}^\dagger(\tau) c_{ib}(\tau') \right\}. \tag{12}$$

Now we study the saddle point of this action in the large-N limit. After integrating out the fermion field and taking $\frac{\delta S}{\delta P_{ba}} = 0$, we obtain

$$P_{ab}(\tau,\tau') = \frac{1}{N} \langle c_{ia}^\dagger(\tau) c_{ib}(\tau') \rangle. \tag{13}$$

Note that we have combined $\frac{N}{2} Q_{ab} |P_{ab}|^2$ and $\frac{N}{2} Q_{ba} |P_{ba}|^2$ as one term. Similarly, taking the derivative with respect to Q_{ab}, we have

$$Q_{ab}(\tau,\tau') = J^2 |P_{ab}(\tau,\tau')|^2. \tag{14}$$

If we only consider the diagonal solution in the replica space (non-spin-glass state), we can define the self-energy

$$\Sigma(\tau,\tau') = -Q(\tau,\tau') P(\tau',\tau) \tag{15}$$

and the Green's function

$$G(\tau,\tau') = -\langle T_\tau c(\tau) c^\dagger(\tau') \rangle. \tag{16}$$

Then we have

$$P(\tau,\tau') = G(\tau',\tau), \tag{17}$$

and the saddle-point solution becomes

$$G(i\omega_n) = \frac{1}{i\omega_n + \mu - \Sigma(i\omega_n)}, \qquad \Sigma(\tau) = -J^2 G^2(\tau) G(-\tau). \tag{18}$$

The above equation shows a reparametrization symmetry at low temperature if we ignore the $i\omega_n$ term [9,10]. At zero temperature, the low-energy Green's function is found to be [1,10]

$$G(z) = C \frac{e^{-i(\pi/4+\theta)}}{\sqrt{z}}, \ \mathrm{Im}(z) > 0, \ |z| \ll J, \ T = 0, \tag{19}$$

where C is a positive number and $-\pi/4 < \theta < \pi/4$ characterizes the particle-hole asymmetry. A full numerical solution for Eq. (18) at zero temperature was also obtained in Ref. [1] and is shown in Fig. 1. We can see the $1/\sqrt{z}$ behavior at low energy. However, it is not possible to work entirely within this low-energy scaling limit to obtain other low-temperature

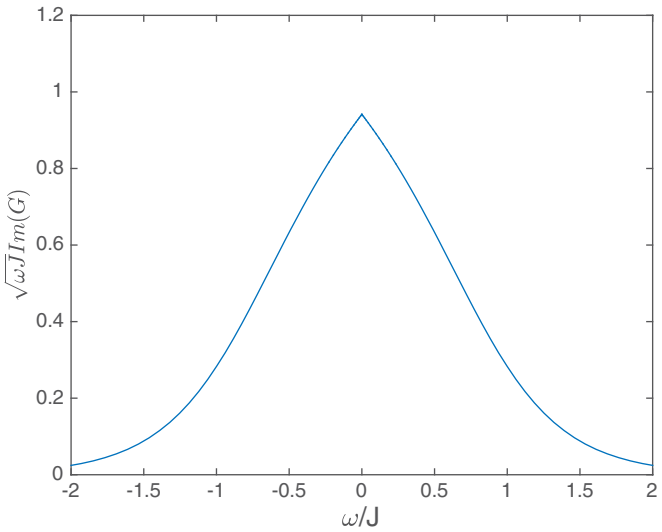

FIG. 1. Plot, adapted from Ref. [1], showing the imaginary part of the Green's function multiplied by $\sqrt{\omega}$ as a function of ω at the particle-hole symmetric point $\theta = 0$. Our definition of the Green's function, Eq. (16), differs by a sign from Ref. [1].

properties: the $i\omega_n$ term is needed to properly regularize the ultraviolet and select among the many possible solutions of the low-energy equations [4,10].

A. Free energy and thermal entropy

The free energy is defined to be

$$\mathcal{F} = -\frac{1}{\beta}\ln \mathcal{Z}_{\rm eff}, \tag{20}$$

where $\mathcal{Z}_{\rm eff}$ has only one replica. So

$$\mathcal{Z}_{\rm eff} = \int Dc^\dagger Dc \exp(-\mathcal{S}), \tag{21}$$

with

$$\mathcal{S} = \sum_i \int_0^\beta d\tau c_i^\dagger \left(\frac{\partial}{\partial\tau} - \mu\right) c_i + \int_0^\beta d\tau d\tau' \times \left\{\frac{N}{4J^2}[Q(\tau,\tau')]^2 + \frac{N}{2}Q(\tau,\tau')|P(\tau,\tau')|^2 - Q(\tau,\tau')P(\tau',\tau)\sum_i c_i^\dagger(\tau)c_i(\tau')\right\}. \tag{22}$$

For the free-energy density $\mathcal{F}/N$, we can just drop the site index i to give the single-site action, substituting the Green's function and self-energy

$$\mathcal{S} = \int_0^\beta d\tau d\tau' c^\dagger(\tau)\left(\frac{\partial}{\partial\tau}\delta(\tau-\tau') - \mu\delta(\tau-\tau') + \Sigma(\tau,\tau')\right)c(\tau') + \int_0^\beta d\tau d\tau' \left\{\frac{1}{4J^2}[\Sigma(\tau,\tau')/G(\tau,\tau')]^2 - \frac{1}{2}\Sigma(\tau,\tau')G(\tau',\tau)\right\}. \tag{23}$$

After integrating out the fermion field

$$\mathcal{S} = -\,\mathrm{Tr}\ln[(\partial_\tau - \mu)\delta(\tau-\tau') + \Sigma(\tau,\tau')] + \int_0^\beta d\tau d\tau' \left\{\frac{1}{4J^2}[\Sigma(\tau,\tau')/G(\tau,\tau')]^2 - \frac{1}{2}\Sigma(\tau,\tau')G(\tau',\tau)\right\}. \tag{24}$$

To verify this result, we can vary with respect to $\Sigma(\tau,\tau')$ and $G(\tau,\tau')$, also using the fact that $\Sigma(\tau,\tau') = \Sigma^*(\tau',\tau)$, $G(\tau,\tau') = G^*(\tau',\tau)$, to obtain the equations of motions as before.

In the large-N limit, we can substitute in the classical solution, and then the free-energy density is

$$\frac{\mathcal{F}}{N} = T\sum_n \ln[-\beta G(i\omega_n)] - \int_0^\beta d\tau \frac{3}{4}\Sigma(\tau)G(-\tau). \tag{25}$$

The thermal entropy density can be obtained by

$$\frac{S}{N} = -\frac{1}{N}\frac{\partial\mathcal{F}}{\partial T}. \tag{26}$$

B. High-temperature expansion

Now we present a solution of Eqs. (18) by a high-temperature expansion (HTE). Equivalently, this can be viewed as an expansion in powers of J.

We will limit ourselves to the simpler particle-hole symmetric case, $\mathcal{Q} = 1/2$, for which both G and Σ are odd functions of ω_n. We start with the high-temperature limit

$$G_0(i\omega_n) = \frac{1}{i\omega_n} \tag{27}$$

and then expand both G and Σ in powers of J^2: $G = G_0 + G_1 + \cdots$ and $\Sigma = \Sigma_0 + \Sigma_1 + \cdots$. The successive terms can be easily obtained by iteratively expanding both equations in Eq. (18) and repeatedly performing Fourier transforms between frequency and time:

$$\begin{aligned}
\Sigma_1(i\omega_n) &= J^2\frac{1}{4i\omega_n},\\
G_1(i\omega_n) &= J^2\frac{1}{4(i\omega_n)^3},\\
\Sigma_2(i\omega_n) &= J^4\frac{3}{16(i\omega_n)^3},\\
G_2(i\omega_n) &= J^4\frac{1}{4(i\omega_n)^5},\\
\Sigma_3(i\omega_n) &= J^6\left[\frac{15}{32(i\omega_n)^5} + \frac{3}{128T^2(i\omega_n)^3}\right],\\
G_3(i\omega_n) &= J^6\left[\frac{37}{64(i\omega_n)^7} + \frac{3}{128T^2(i\omega_n)^5}\right],\\
\Sigma_4(i\omega_n) &= J^8\left[\frac{561}{256(i\omega_n)^7} + \frac{75}{512T^4(i\omega_n)^5} - \frac{1}{256T^4(i\omega_n)^3}\right],\\
G_4(i\omega_n) &= J^8\left[\frac{5}{2(i\omega_n)^9} + \frac{81}{512T^2(i\omega_n)^7} - \frac{1}{256T^4(i\omega_n)^5}\right].
\end{aligned} \tag{28}$$

The free-energy density can be written in terms of $G(i\omega_n)$ and $\Sigma(i\omega_n)$:

$$\frac{\mathcal{F}}{N} = T\sum_n \ln\left[-\beta G(i\omega_n)\right] - \frac{3T}{4}\sum_n \Sigma(i\omega_n)G(i\omega_n). \tag{29}$$

We also need to regularize the above free energy by subtracting and adding back the free-particle part:

$$\frac{\mathcal{F}}{N} = -T\ln 2 + T\sum_n \{\ln\left[-\beta G(i\omega_n)\right] - \ln(-\beta i\omega_n)\} - \frac{3T}{4}\sum_n \Sigma(i\omega_n)G(i\omega_n). \tag{30}$$

The series expansion of the entropy density is

$$\frac{\mathcal{S}}{N} = \ln 2 - \frac{1}{64}\frac{J^2}{T^2} + \frac{1}{512}\frac{J^4}{T^4} - \frac{11}{36864}\frac{J^6}{T^6} + \frac{599}{11796480}\frac{J^8}{T^8} + \cdots. \tag{31}$$

Next, we describe our numerical solution of Eq. (18) at nonzero temperature. We used a Fourier transform (FT) to iterate between the two equations, until we obtained a convergent solution. For faster convergence, we started at high temperature, and used the above high-temperature expansion as the initial form. Then we decreased temperature to get the full temperature dependence. We compare the large-N exact numerical result with the high-temperature expansion in Fig. 2. At high temperatures, all methods converge to $\ln 2$ as expected. The HTE results fit the exact numerics quite well for $T/J > 0.6$, but are no longer accurate at lower T. The exact numerics shows a finite entropy density in the limit of vanishing temperature, with a value consistent with earlier analytic results [4,10].

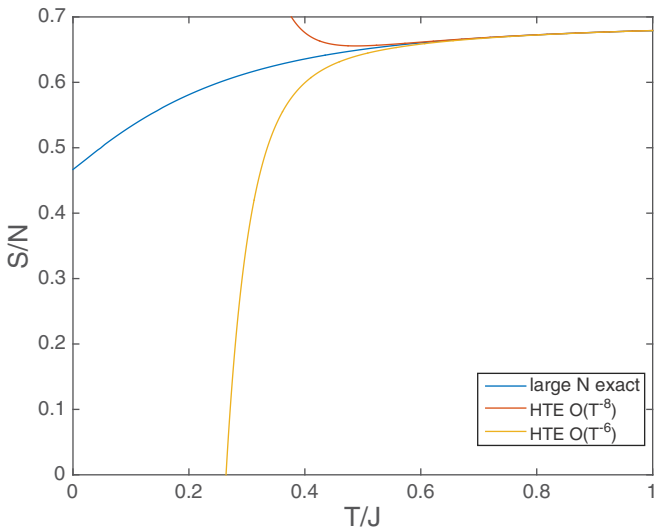

FIG. 2. Entropy computation from exact large-N EOM and HTE: at high temperature, all approach the infinite-temperature limit $S/N = \ln 2$. HTE result fits the exact result quite well for $T/J > 0.6$.

III. EXACT DIAGONALIZATION FOR FERMIONS

We now test the validity of the large-N results by comparing with an exact-diagonalization (ED) computation at finite N. For the numerical setup, it was useful to employ the Jordan-Wigner transformation to map the Hamiltonian to a spin model:

$$c_i = \sigma_i^- \prod_{j<i}\sigma_j^z, \quad c_i^\dagger = \sigma_i^+ \prod_{j<i}\sigma_j^z. \tag{32}$$

We built a matrix of the N spins and diagonalized it numerically. After obtaining the full spectrum, we obtained both the imaginary part of the Green's function and thermal entropy, and our results are compared with the large-N results in Fig. 1 and Fig. 2.

In this note, we focus on the particle-hole symmetric point. But particle-hole symmetry does not correspond to the point $\mu = 0$ in the Hamiltonian Eq. (1), because there are quantum corrections to the chemical potential $\delta\mu \sim O(N^{-1})$ coming from the terms in which i,j,k,l are not all different from each other, because these terms are not particle-hole symmetric. So we use a Hamiltonian with extra correction terms that compensate $\delta\mu$:

$$H = \frac{1}{(2N)^{3/2}}\sum_{i,j,k,\ell=1}^{N} J_{ij;k\ell}\,(c_i^\dagger c_j^\dagger c_k c_\ell + \delta_{ik}n\, c_j^\dagger c_l - \delta_{il}n\, c_j^\dagger c_k - \delta_{jk}n\, c_i^\dagger c_l + \delta_{jl}n\, c_i^\dagger c_k), \tag{33}$$

where we use $n = 1/2$ for the particle-hole symmetric case.

We define the on-site retarded Green's function by

$$G_i^R(t,t') = -i\theta(t-t')\langle\{c_i(t), c_i^\dagger(t')\}\rangle. \tag{34}$$

Using the Lehmann representation

$$G_i^R(\omega) = \frac{1}{Z}\sum_{nn'}\frac{\langle n|c_i|n'\rangle\langle n'|c_i^\dagger|n\rangle}{\omega + E_n - E_{n'} + i\eta}(e^{-\beta E_n} + e^{-\beta E_{n'}}) \tag{35}$$

at zero temperature, we obtain

$$G_i^R(\omega) = \sum_{n'}\frac{\langle 0|c_i|n'\rangle\langle n'|c_i^\dagger|0\rangle}{\omega + E_0 - E_{n'} + i\eta} + \frac{\langle 0|c_i^\dagger|n'\rangle\langle n'|c_i|0\rangle}{\omega - E_0 + E_{n'} + i\eta}. \tag{36}$$

Using $(\omega + i\eta)^{-1} = \mathcal{P}\frac{1}{\omega} - i\pi\delta(\omega)$,

$$\mathrm{Im}G_i^R(\omega) = -\pi\sum_{n'}[\langle 0|c_i|n'\rangle\langle n'|c_i^\dagger|0\rangle\delta(\omega + E_0 - E_{n'}) + \langle 0|c_i^\dagger|n'\rangle\langle n'|c_i|0\rangle\delta(\omega - E_0 + E_{n'})]. \tag{37}$$

Numerically, we replace the delta function with a Lorentzian by taking a small η:

$$\delta(E_0 - E_{n'} + \omega) = \lim_{\eta\to 0^+}\frac{1}{\pi}\frac{\eta}{(E_0 - E_{n'} + \omega)^2 + \eta^2}. \tag{38}$$

A subtlety in the above numerics, when $\mu = 0$, is the presence of an antiunitary particle-hole symmetry. The ground state turns out to be doubly degenerate for some system sizes. If so, we will have two ground states $|0\rangle$ and $|0'\rangle$ in the expression of $G_i^R(\omega)$, and we need to sum them up to get the correct Green's function.

To better understand this degeneracy, we can define the particle-hole transformation operator

$$P = \prod_i (c_i^\dagger + c_i) K, \tag{39}$$

where K is the antiunitary operator. One can show that it is a symmetry of our Hamiltonian Eq. (33), $[H, P] = 0$. When the total site number N is odd, we know any eigenstate $|\Psi\rangle$ and its particle-hole partner $P|\Psi\rangle$ must be different and degenerate. For even site number, these two states may be the same state. However for $N = 2 \mod 4$, one can show that $P^2 = -1$, and then the degeneracy is analogous to the time-reversal Kramers doublet for $T^2 = -1$ particles. We expect that all the eigenvalues must be doubly degenerate. For $N = 0 \mod 4$, $P^2 = 1$, there is no protected degeneracy in the half-filling sector. These facts were all checked by numerics, and carefully considered in the calculation of the Green's function.

A better understanding of the above facts can be reached from the perspective of symmetry-protected topological (SPT) phases. As shown recently in Ref. [14], the complex SYK model can be thought of as the boundary of a 1D SPT system in the symmetry class AIII. The periodicity of 4 in N arises from the fact that we need to put 4 chains to gap out the boundary degeneracy without breaking the particle-hole symmetry. In the Majorana SYK case, the symmetric Hamiltonian can be constructed as a symmetric matrix in the Clifford algebra $Cl_{0,N-1}$, and the Bott periodicity in the real representation of the Clifford algebra gives rise to a $\mathbb{Z}_8$ classification [14]. Here, for the complex SYK case, we can similarly construct the Clifford algebra by dividing one complex fermion into two Majorana fermions, and then we will have a periodicity of 4.

A. Green's function

From the above definition of the retarded Green's function, we can relate them to the imaginary-time Green's function as defined in Eq. (16), $G^R(\omega) = G(i\omega_n \to \omega + i\eta)$. In Fig. 3, we

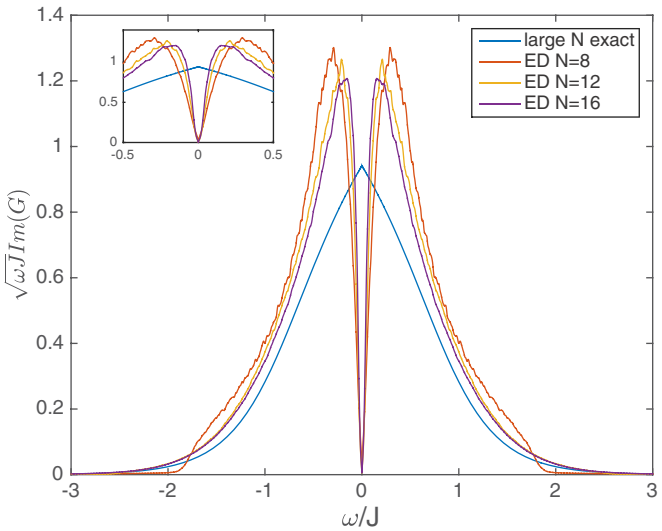

FIG. 3. Imaginary part of the Green's function in real frequency space from large N and exact diagonalization. The inset figure is zoomed in near $\omega = 0$.

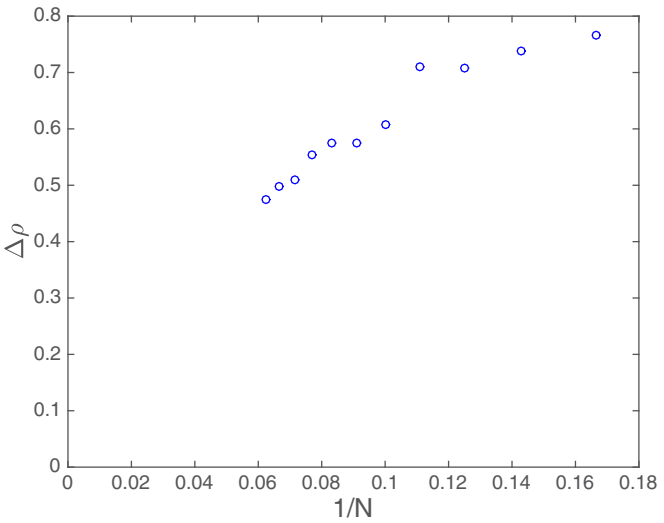

FIG. 4. The difference of integrated spectral function between ED at different N and large-N result. The difference appears to be tending to 0 as N approaches infinity.

show a comparison between the imaginary part of the Green's function from large N, and from the exact-diagonalization computation. The spectral function from ED is particle-hole symmetric for all N; this is guaranteed by the particle-hole symmetry and can be easily shown from the definition of the spectral function Eq. (37). The two results agree well at high frequencies. At low frequencies, the deviations between the exact-diagonalization and large-N results get smaller at larger N.

For a quantitative estimate of the deviations between the large-N and exact-diagonalization results, we we compute the areas under each curve in Fig. 3, and compare their difference:

$$\Delta\rho = \int d\omega |\mathrm{Im}G_{ED}(\omega) - \mathrm{Im}G_{N=\infty}(\omega)|. \tag{40}$$

As shown in Fig. 4, the convergence to the $N = \infty$ limit is slow, possibly with a power smaller than $1/N$.

B. Entropy

We can also compute the finite-temperature entropy from ED. The partition function can be obtained from the full spectrum

$$\mathcal{Z} = \sum_n e^{-\beta E_n}, \tag{41}$$

where E_n is the many-body energy, and then free energy density is

$$\frac{F}{N} = -\frac{\beta}{N} \log \mathcal{Z}. \tag{42}$$

We can obtain the entropy density from

$$\frac{S}{N} = \frac{1}{N} \frac{\langle E \rangle - F}{T}, \tag{43}$$

where $\langle E \rangle = \sum_n \frac{E_n e^{-\beta E_n}}{\mathcal{Z}}$ is the average energy.

We use this approach to compute the thermal entropy from the full spectrum, and compare it with the thermal entropy

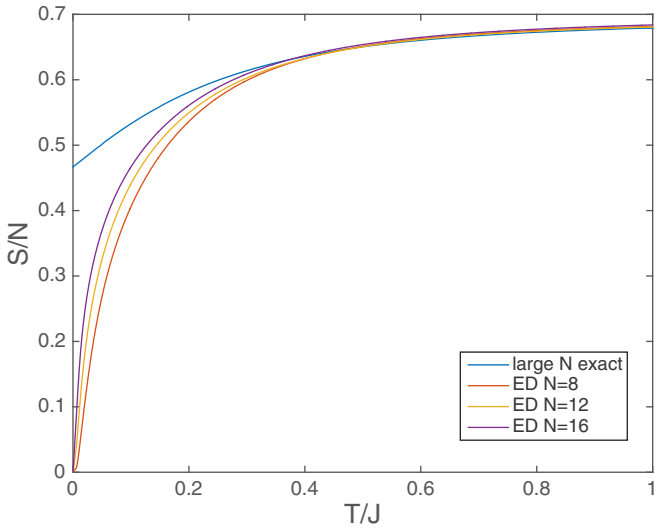

FIG. 5. Thermal entropy computation from ED, and large N. At high temperature, all results approach the infinite-temperature limit $S/N = \ln 2$. At low temperature, all ED results go to zero, but do approach the $N = \infty$ results with increasing N. Note that the limits $N \to \infty$ and $T \to 0$ do not commute, and the nonzero entropy as $T \to 0$ is obtained only when the $N \to \infty$ is taken first.

calculated from large-N equations of motion Eq. (18). As shown in Fig. 5, the finite-size ED computation gives rise to the correct limit $s = \ln 2$ in the high-temperature regime, and it agrees with the large-N result quite well for $T/J > 0.5$. Although there is a clear trend that a larger system size gives rise to larger thermal entropy at low temperature, we cannot obtain a finite zero-temperature entropy for any finite N. This is due to the fact that the nonzero zero-temperature entropy is obtained by taking the large-N limit first then taking the zero-temperature limit.

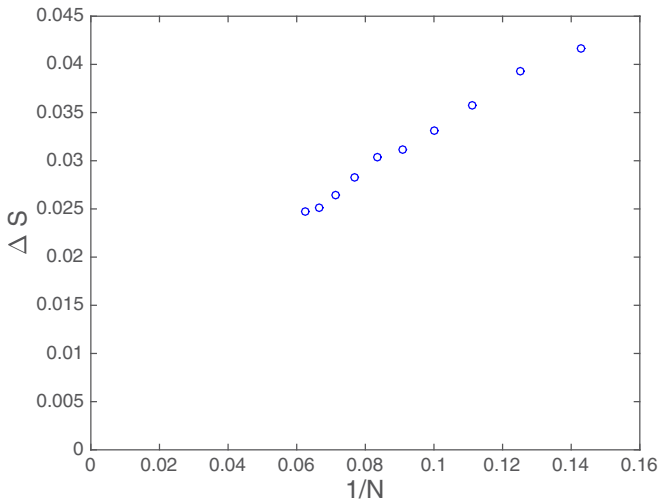

FIG. 6. The difference of integrated thermal entropy between ED at different N and large-N result. The difference goes to 0 as $1/N$ approaches 0.

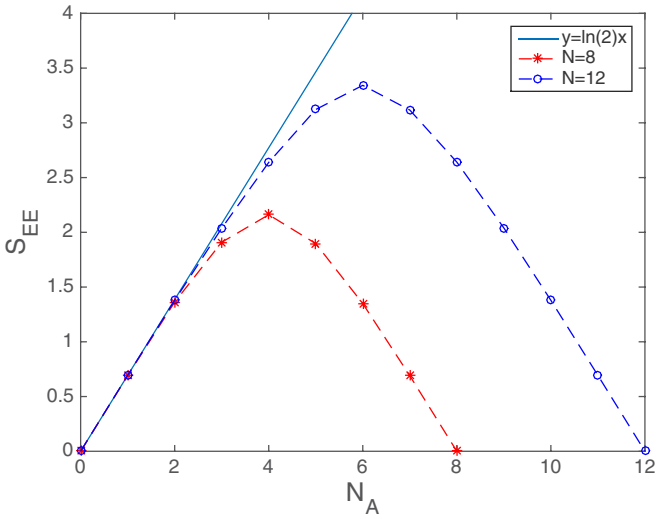

FIG. 7. Entanglement entropy for the ground state. We divide the system into two subsystems, A and B, and we trace out part B and calculate the entropy for the reduced density matrix ρ_A. The x axis is the size of subsystem A.

As in Fig. 4, we estimate the deviation from the large-N theory by defining

$$\Delta S = \int dT |S_{ED}(T)/N - S_{N=\infty}(T)/N_\infty|, \qquad (44)$$

and plot the result in Fig. 6. The finite-size correction goes to 0 as $1/N$ goes to zero.

C. Entanglement entropy

Finally, we compute the entanglement entropy in the ground state, obtained by choosing a subsystem A of N sites, and tracing over the remaining sites; the results are in Fig. 7. For $N_A < N/2$, we find that S_{EE} is proportional to N_A, thus obeying the volume law, and so even the ground state obeys eigenstate thermalization [14]. We would expect that S_{EE}/N_A equals the zero-temperature limit of the entropy density S/N [18]. However, our value of S_{EE}/N_A appears closer to $\ln 2$ (see Fig. 7) than the value of S/N as $T \to 0$. Given the small difference between $\ln 2 = 0.69$ and $S/N(T \to 0) = 0.464848\ldots$, we expect that this is a finite-size discrepancy.

IV. OUT-OF-TIME-ORDER CORRELATIONS AND SCRAMBLING

One of the interesting properties of the SYK model is that it exhibits quantum chaos [9,13]. The quantum chaos can be quantified in terms of an out-of-time-ordered correlator $\langle A(t)B(0)A(t)B(0)\rangle$ (OTOC) obtained from the cross terms in $\langle [A(t), B(0)]^2\rangle$ [11]. The exponential decay in the OTOC results in an exponential growth of $\langle [A(t), B(0)]^2\rangle$ at short times, and the latter was connected to analogous behavior in classical chaos. In particular, Ref. [11] established a rigorous bound, $2\pi/\beta$, for the decay rate, λ_L, of the OTOC, and the Majorana SYK model is expected [9] to saturate this bound in the strong-coupling limit $\beta J \gg 1$. In the opposite perturbative limit, $\beta J \ll 1$, one expects $\lambda_L \sim J$. The authors of Ref. [12]

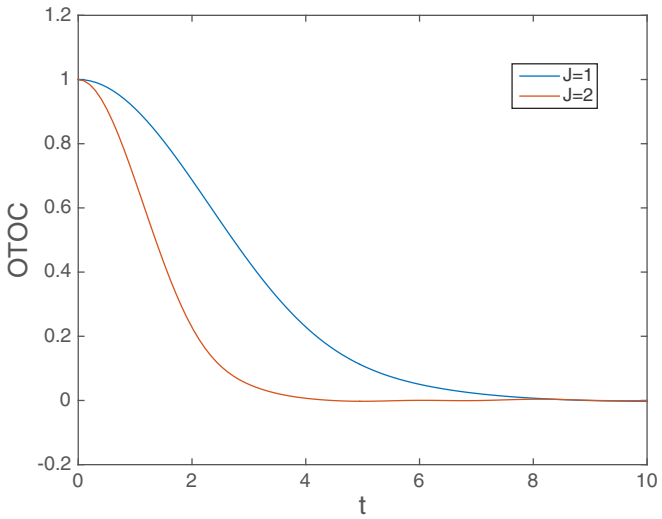

FIG. 8. OTOC as a function of time at infinite temperature with different interaction strength $J = 1$ and $J = 2$. Here the total system size $N = 7$.

performed an ED calculation of the OTOC on the Majorana SYK model in the infinite-temperature limit, $\beta = 0$. Here we will perform a similar calculation on the complex SYK model, and also obtain results at large βJ. We define our renormalized OTOC by

$$\text{OTOC} = -\frac{\langle A(t)B(0)A(t)B(0)\rangle + \langle B(0)A(t)B(0)A(t)\rangle}{2\langle AA\rangle\langle BB\rangle}. \tag{45}$$

We choose the Hermitian Majorana operators $A = c_1 + c_1^\dagger$, $B = c_2 + c_2^\dagger$. The negative sign gives a positive initial value for OTOC. At infinite temperature, the result is shown in Fig. 8. We observe the fast-scrambling effect from the quick decay of OTOC, and the early-time decay rate λ_L is proportional to J as expected. Similar behavior is found in the Majorana SYK model [12]. At finite temperature, although we can perform the computation in the strong-coupling limit $\beta J \gg 1$, because of finite-size effects, we do not get the predicted decay rate $\lambda_L = 2\pi/\beta$. And the OTOC only has a weak dependence on β even in the strong-coupling limit as shown in Fig. 9. Theoretically [9,11], in the large-N and strong-coupling conformal limit $N \gg \beta J \gg 1$, during the scrambling process $\beta \ll t < \beta \log N$, we have $1 - \text{OTOC} \sim (\beta J/N)e^{(2\pi/\beta)t}$. Because of numerical computation power constraints, we cannot reach the large-N conformal limit, and therefore we do not have a well-defined scrambling period. As a consequence, Fig. 9 does not display a large change in the exponent, and the prefactor difference is also small. It is clearly that of our small system sizes, J is the most relevant energy scale for controlling the chaos.

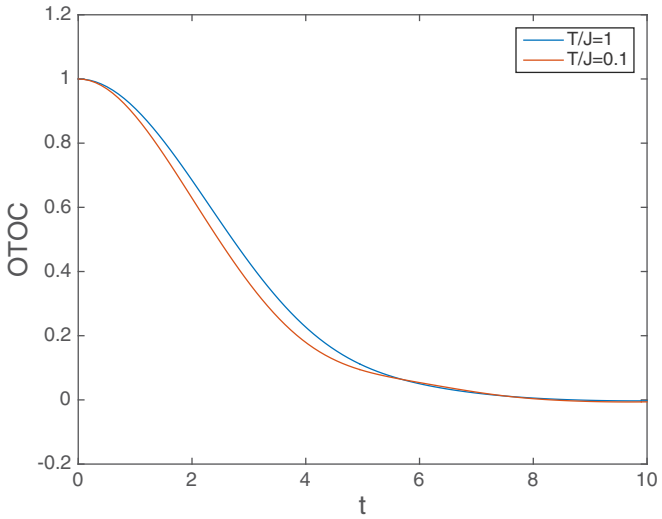

FIG. 9. OTOC as a function of time at different temperature with interaction strength $J = 1$. Here the total system size $N = 7$.

V. SYK MODEL FOR BOSONS

Now we consider a "cousin" of the present model: the SYK model for hard-core bosons. The bosonic case was also considered in the early work [1–4] but with a large number of bosons on each site. It was found that over most of the parameter regime the ground state had spin-glass order. We will find evidence of similar behavior here.

The Hamiltonian will be quite similar to Eq. (1), except that because of the Bose statistics now the coefficients obey

$$J_{ji;kl} = J_{ij;kl},\ J_{ij;lk} = J_{ij;kl},\ J_{kl;ij} = J^*_{ij;kl}. \tag{46}$$

The hard-core boson satisfies $[b_i, b_j] = 0$ for $i \neq j$ and $\{b_i, b_i^\dagger\} = 1$. Also to make particle-hole symmetry (39) hold, we only consider pair hopping between different sites; i.e., site indices i, j, k, l are all different, and we drop the normal order correction terms. The spin formalism in ED will be even simpler, as we do not need to attach a Jordan-Wigner string of σ_z:

$$b_i = \sigma_i^-, \quad b_i^\dagger = \sigma_i^+. \tag{47}$$

We can define a similar Green's function for bosons:

$$G_B(t) = -i\theta(t)\langle\{b(t), b^\dagger(0)\}\rangle. \tag{48}$$

We identify the infinite-time limit of G_B as the Edward-Anderson order parameter q_{EA}, which can characterize the long-time memory of spin glass:

$$q_{EA} = \lim_{t\to\infty} G_B(t). \tag{49}$$

Then $q_{EA} \neq 0$ indicates that $G_B(\omega) \sim \delta(\omega)$. This is quite different from the fermionic case, where we have $G_F(z) \sim 1/\sqrt{z}$; this inverse square-root behavior also holds in the bosonic case without spin-glass order [1]. Figure 10 is our result from ED, with a comparison between G_B with G_F. It is evident that the behavior of G_B is qualitatively different from G_F, and so an inverse square-root behavior is ruled out. Instead, we can clearly see that, as system size gets larger, G_B's peak value increases much faster than G_F's peak value. This supports the presence of spin-glass order.

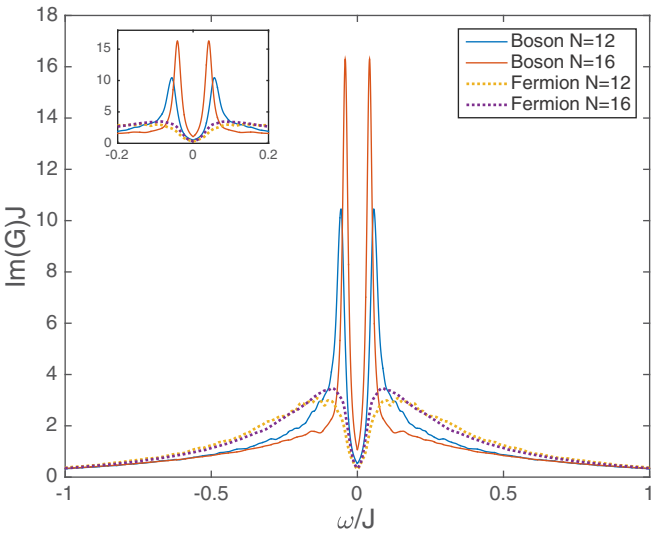

FIG. 10. Imaginary part of Green's function for hard-core boson and fermion model. The peak near the center gets much higher in the boson model when system size gets larger. The inset figure is zoomed in near $\omega = 0$.

Unlike the fermionic case, $P^2 = 1$ for all N in the bosonic model. We can apply a symmetry argument similar to that in Ref. [14]: for the half-filled sector (only in even-N cases), the level statistics obeys the Wigner-Dyson distribution of Gaussian orthogonal random matrix ensembles, while in other filling sectors, it obeys distribution of Gaussian unitary random matrix ensembles.

Our thermal entropy results for bosons are similar to the fermionic results: although the entropy eventually approaches 0 at zero temperature, there is still a trend of a larger low-temperature entropy residue as the system size gets larger.

We have also computed the entanglement entropy for the ground state of the hard-core boson SYK model. It still satisfies volume law, and the entanglement entropy density is still quite close to $\ln 2$. Finally results for the OTOC are qualitatively similar to the fermionic results.

VI. CONCLUSIONS

We have presented exact-diagonalization results on the fermionic SYK model. The trends in the computed Green's functions, high-temperature expansion, entropy density, and entanglement entropy all support the conclusion that the large-N limit approaches the compressible non-Fermi-liquid state obtained in the earlier $N = \infty$ analysis. Note that the entropy density approaches a nonzero value in the limit $T \to 0$ taken *after* the $N \to \infty$, and so the ground state itself exhibits eigenstate thermalization. This conclusion is also supported by the volume-law behavior of the entanglement entropy. The original model of Ref. [1] was argued [4] to have an instability to spin-glass order at temperatures exponentially small in $\sqrt{M}$; the consonance between large-N theory and our finite-N numerics indicates that the model in (1) (with a random interaction with 4 indices [9]) does not have such an instability.

For the SYK model for hard-core bosons, our results for the single-particle Green's function were very different, and indicate the presence of spin-glass order. Similar quantum spin-glass states were examined in random models of bosons in Refs. [3,4].

ACKNOWLEDGMENTS

We thank Kartiek Agarwal, Shiang Fang, Tarun Grover, Yingfei Gu, Steve Gubser, Steve Shenker, and Yi-Zhuang You for valuable discussions. This research was supported by the NSF under Grant No. DMR-1360789 and MURI Grant No. W911NF-14-1-0003 from ARO. Research at Perimeter Institute is supported by the Government of Canada through Industry Canada and by the Province of Ontario through the Ministry of Research and Innovation.

[1] S. Sachdev and J. Ye, Gapless Spin-Fluid Ground State in a Random Quantum Heisenberg Magnet, Phys. Rev. Lett. **70**, 3339 (1993).
[2] O. Parcollet and A. Georges, Non-Fermi-liquid regime of a doped Mott insulator, Phys. Rev. B **59**, 5341 (1999).
[3] A. Georges, O. Parcollet, and S. Sachdev, Mean Field Theory of a Quantum Heisenberg Spin Glass, Phys. Rev. Lett. **85**, 840 (2000).
[4] A. Georges, O. Parcollet, and S. Sachdev, Quantum fluctuations of a nearly critical Heisenberg spin glass, Phys. Rev. B **63**, 134406 (2001).
[5] L. Arrachea and M. J. Rozenberg, Infinite-range quantum random Heisenberg magnet, Phys. Rev. B **65**, 224430 (2002).
[6] A. Camjayi and M. J. Rozenberg, Quantum and Thermal Fluctuations in the SU(N) Heisenberg Spin-Glass Model near the Quantum Critical Point, Phys. Rev. Lett. **90**, 217202 (2003).
[7] S. Sachdev, Holographic Metals and the Fractionalized Fermi Liquid, Phys. Rev. Lett. **105**, 151602 (2010).
[8] S. Sachdev, Strange metals and the AdS/CFT correspondence, J. Stat. Mech. (2010) P11022.
[9] A. Y. Kitaev, A simple model of quantum holography, in KITP strings seminar and Entanglement 2015 program, UC Santa Barbara, Santa Barbara USA, 12 February, 7 April and 27 May 2015, http://online.kitp.ucsb.edu/online/entangled15/.
[10] S. Sachdev, Bekenstein-Hawking Entropy and Strange Metals, Phys. Rev. X **5**, 041025 (2015).
[11] J. Maldacena, S. H. Shenker, and D. Stanford, A bound on chaos, arXiv:1503.01409.

[12] P. Hosur, X.-L. Qi, D. A. Roberts, and B. Yoshida, Chaos in quantum channels, J. High Energy Phys. 02 (2016) 004.

[13] J. Polchinski and V. Rosenhaus, The Spectrum in the Sachdev-Ye-Kitaev Model, J. High Energy Phys. 04 (2016) 001.

[14] Y.-Z. You, A. W. W. Ludwig, and C. Xu, Sachdev-Ye-Kitaev model and thermalization on the boundary of many-body localized fermionic symmetry protected topological states, arXiv:1602.06964.

[15] D. Anninos, T. Anous, and F. Denef, Disordered quivers and cold horizons, arXiv:1603.00453.

[16] A. Jevicki, K. Suzuki, and J. Yoon, Bi-local holography in the SYK model, arXiv:1603.06246.

[17] O. DeWolfe, S. S. Gubser, and C. Rosen, Fermi Surfaces in Maximal Gauged Supergravity, Phys. Rev. Lett. **108**, 251601 (2012).

[18] We thank Tarun Grover and Yi-Zhuang You for pointing this out to us.